REPORT DOCUMENTATION PAGE

Form Approved
OMB No. 0704-0188

PLEASE DO NOT RETURN YOUR FORM TO THE ABOVE ORGANIZATION.

1. REPORT DATE *(DD-MM-YYYY)*	2. REPORT TYPE	3. DATES COVERED *(From - To)*
24-02-2014	Final	01/03/09 to 28/02/14

4. TITLE AND SUBTITLE

Fast response and low voltage dual frequency liquid crystals

5a. CONTRACT NUMBER

5b. GRANT NUMBER

FA9550-09-1-0170

5c. PROGRAM ELEMENT NUMBER

6. AUTHOR(S)

Shin-Tson Wu

5d. PROJECT NUMBER

5e. TASK NUMBER

5f. WORK UNIT NUMBER

7. PERFORMING ORGANIZATION NAME(S) AND ADDRESS(ES)

University of Central Florida, Office of Research and Commercialization
12201 Research Parkway, Suite 501
Orlando, FL 32826

8. PERFORMING ORGANIZATION REPORT NUMBER

Final

9. SPONSORING/MONITORING AGENCY NAME(S) AND ADDRESS(ES)

Air Force Office of Scientific Research/RTD
875 N. Randolph Street, Suite 325, Room 3112
Arlington, VA 22203

10. SPONSOR/MONITOR'S ACRONYM(S)

AFOSR

11. SPONSOR/MONITOR'S REPORT NUMBER(S)

Final

12. DISTRIBUTION/AVAILABILITY STATEMENT

Approved for public release; distribution is unlimited.

13. SUPPLEMENTARY NOTES

14. ABSTRACT

Two types of liquid crystal phase modulators: dual frequency liquid crystal (DFLC) and polymer network liquid crystal (PNLC) with 2-pi phase change and submillisecond response time were demonstrated. For DFLC, a record-high birefringence DFLC, an ultra-low crossover frequency DFLC (UCF-01), and a high figure-of-merit DFLC (UCF-02) intended for elevated temperature operation were developed. The figure-of-merit of UCF-02 is 5X higher than that of Merck MLC-2048. For PNLC, a PNLC phase modulator with low scattering (<3%) at λ=1.06 μm was demonstrated. The operating voltage for 2-pi phase change is ~70V at room temperature, and the relaxation time is 220 μs at 25°C and 30 μs at 70°C. Finally, a partially fluorinated terphenyl liquid crystal with low absorption in both mid-wave infrared (MWIR) and near IR regions was synthesized. This compound exhibits a nematic phase (although only 2°C), reasonably high birefringence (0.2), low visco-elastic coefficient, and modest dielectric anisotropy. This compound serves as an important first example for future development of low-loss MWIR liquid crystals.

15. SUBJECT TERMS

Dual frequency liquid crystal, polymer network liquid crystal, submillisecond response time, low-loss infrared liquid crystal

16. SECURITY CLASSIFICATION OF:			17. LIMITATION OF ABSTRACT	18. NUMBER OF PAGES	19a. NAME OF RESPONSIBLE PERSON
a. REPORT	b. ABSTRACT	c. THIS PAGE	UU	21	Shin-Tson Wu
					19b. TELEPHONE NUMBER *(Include area code)* 407-823-4763

Reset

AFOSR Final Report

Fast Response and Low Voltage Dual Frequency Liquid Crystals

Contract No. FA9550-09-1-0170
UCF Project No. 6501-6182

Prepared for: Dr. Charles Y-C Lee
AFOSR/RTD
875 North Randolph Street
Suite 325, Room 3112
Arlington, VA 22203
Phone: (703) 696-7779
Fax: (703) 696-8449
Email: charles.lee.21@us.af.mil

Principal Investigator: Prof. Shin-Tson Wu
College of Optics and Photonics
University of Central Florida
Telephone: (407) 823-4763
Email: swu@ucf.edu

Contract Period: March 1, 2009 to Feb. 28, 2014

Fast Response and Low Voltage Dual Frequency Liquid Crystals

1. Objectives:

The objective of this program is to develop high performance dual-frequency liquid crystal (DFLC) mixtures and employing DFLC to develop fast response electro-optical devices with low switching voltage. High performance DFLC mixture requires low crossover frequency, high birefringence, large dielectric anisotropy at both low frequency and high frequency limits, and low viscosity. Appropriate device configuration also helps to lower the switching voltage while maintaining a fast response time.

2. Status of Effort:

In this performance period, we have developed: 1) high performance DFLC mixtures, 2) submillisecond-response and scattering-free polymer network liquid crystals for IR laser beam steering, and 3) low absorption loss nematic liquid crystals (LCs) for MWIR applications. We highlight the progress in each category as follows.

2.1 High performance DFLC mixtures with high birefringence (Δn) and ultra-low crossover frequency (f_c). A Merck DFLC mixture MLC-2048 serves as benchmark for comparison; its Δn=0.202 at λ=633 nm and 25 °C, and crossover frequency f_c~18.9 kHz at 20 °C.

1. UCF-DFLC exhibits a record-high birefringence Δn=0.38 at λ=633 nm and 0.33 at λ=1550 nm at 25 °C;
2. UCF-01 is a ultra-low crossover frequency DFLC mixture intended for elevated temperature operation; its crossover frequency is only 5.8 kHz at 45°C and 13.5 kHz at 55°C;
3. Using UCF-01, we demonstrated a submillisecond ($\tau_{on}+\tau_{off}$ <0.8 ms) response time DFLC device with a 2π phase change at λ=1.55 μm and merely 40 V_{rms} operation voltage at 55°C;
4. UCF-02: Δn=0.305 at λ=633nm, 25°C, the crossover frequency at room temperature is only 1.2 kHz and it increases gradually to 17 kHz at 55°C. Under the same crossover frequency limitation, the figure of merit of UCF-02 is 5X higher than that of MLC-2048, which means UCF-02 can achieve more than 5X faster response time than MLC-2048.

2.2 Submillisecond-response and scattering-free polymer network liquid crystals (PNLC) for infrared phase modulators. Our PNLC phase modulator is nearly scattering-free (<3%) at λ=1.06 μm. The operating voltage for 2π phase change is ~70V at room temperature, and the relaxation time is 220 μs at 25°C and 30 μs at 70°C. Compared to previous PNLC phase modulator, the response time is improved by ~4X. If we compare to traditional E7 nematic LC 2π phase modulator (d=12 μm), the improvement is ~1000X. For reflective mode operation, the operation voltage could be further lowered by ~30% for the same amount of phase modulation.

2.3 A partially fluorinated terphenyl liquid crystal with low absorption in both mid-wave infrared (MWIR) and near IR regions. This compound exhibits a nematic phase (although only about 2°C), reasonably high birefringence (Δn~0.2), low visco-elastic coefficient, and modest dielectric anisotropy ($\Delta\varepsilon = -2.7$). This compound serves as an important first example for future development of low-loss MWIR liquid crystals and devices.

3. Accomplishments

3.1 Motivation

(1) The demand for faster response time has DFLC into limelight. The frequency revertible dielectric anisotropy makes it possible to align the DFLC molecules along or perpendicular to the electric field direction by varying the frequency of the driving signals. This makes it possible to accelerate both turn-on and turn-off processes by applying a high voltage pulse with different frequencies. On the other hand, the formulation and operation of DFLC material is highly dependent on the crossover frequency. High crossover frequency will demand a high frequency driving signal to address the DFLC, which in turn increases the complexity and cost of driving circuits, power consumption, and dielectric heating.

(2) PNLC can achieve submillisecond response time while maintaining a large phase shift. It can also generate continuous phase change with a relatively simple driving scheme. The major issue which hinders the widespread application of PNLC as a phase-only modulator is the voltage-on state light scattering caused by LC multi-domains. Although it has been reported that high polymer ratio (60~70%) can result in scattering-free holographic polymer

dispersed liquid crystal (HPDLC) with nanoscale droplet sizes, the required operating voltage is relatively high (15-20 V/μm). For a 20-μm HPDLC device, the required operation voltage is >300 volts, which is not practical.

(3) A major concern for IR applications using LCs is the inherent absorption loss due to the existence of molecular vibration bands. Even in the off-resonance regions, the baseline absorption coefficient may reach as high as $\alpha \sim 10$ cm^{-1}. If the LC layer is thin (~5 μm), then the absorption loss is negligible. However, to achieve a sufficient phase change a minimum cell gap is required. As the cell gap increases, the absorption loss increases exponentially.

3.2 Fast-Response and Low-Voltage Dual Frequency Liquid Crystal (DFLC)

3.2.1 Introduction

In most of nematic LC devices, only the turn-on process can be shortened by increasing the electric field, the turn-off or relaxation process is still governed by the surface anchoring and elastic restoring forces. For a LC modulator operating at an infrared wavelength, a thicker cell gap is required in order to achieve the same phase change according to $\delta = 2\pi d\Delta n/\lambda$, where d is the LC cell gap, Δn is the LC birefringence, and λ is the wavelength. As the LC layer thickness increases, the response time also increases as d^x; where x=2 for the case of strong anchoring and $x \rightarrow 1$ when the anchoring is weak. The demand for faster response time has brought DFLC into limelight.

A DFLC mixture usually consists of both positive dielectric anisotropy ($\Delta\varepsilon$) and negative $\Delta\varepsilon$ LC compounds. The positive compounds exhibit a strong Debye relaxation frequency while the negative compounds are basically independent of frequency up to mega-Hertz region. As a result, the $\Delta\varepsilon$ of a DFLC mixture gradually changes from positive at low frequencies (~1 kHz) to zero, and then negative as frequency keeps increasing (say, 30 kHz). The frequency where $\Delta\varepsilon$=0 is called crossover frequency. For device applications, we can drive the device with a low frequency voltage burst to obtain fast rise time. During relaxation, we apply a high frequency voltage burst to assist the decay process. Therefore, both fast rise and decay time can be achieved. This characteristic is especially helpful for speeding up the response time of IR devices.

3.2.2 Figure-of-Merit of DFLC

To design new DFLC materials, we need to analyze the governing factors which determine the DFLC response time and operating voltage. Let us use a vertical alignment DFLC cell with strong anchoring as an example. If we neglect the flow effect, the LC director's response time can be calculated as follows:

$$\tau_{on} \sim \frac{\tau_o}{\left(V_h / V_{th,h}\right)^2 - 1} \tag{1}$$

$$\tau_{off} \sim \frac{\tau_o}{\left(V_l / V_{th,l}\right)^2 + 1} \tag{2}$$

where

$$\tau_0 = \gamma_1 d^2 / K_{33}\pi^2 \tag{3}$$

In Eqs. (1) to (3), V_h and V_l are the driving voltages at high and low frequencies, $V_{th,h}$ and $V_{th,l}$ are the corresponding threshold voltages, γ_1 is the rotational viscosity, K_{33} is the bend elastic constant, and d is the cell gap. The response time of a homogeneous alignment DFLC cell has similar forms to those shown in Eqs. (1) to (3) by replacing K_{33} with K_{11} (splay elastic constant). If we compare the device performance at the same voltage, wavelength, and phase change, then the contribution solely from material properties can be evaluated by a figure of merit (FoM):

$$\text{FoM}_{\text{DFLC}} \equiv \frac{(\Delta n)^2 K_{ii}}{\gamma_1 V_{th}^2} \tag{4}$$

where K_{ii} is the elastic constant and V_{th} is the threshold voltage corresponding to the cell configuration. The dielectric anisotropy of DFLC is frequency dependent. Thus, the threshold voltage and consequently the figure of merit also depend on the frequency and waveform of the driving voltage. If the driving signal is sinusoidal, the elastic constant in Eq. (4) can be cancelled and the FoM leads to:

$$\mathrm{FoM}_{\mathrm{DFLC}} = \frac{(\Delta n)^2 \Delta\varepsilon\varepsilon_0}{\gamma_1 \pi^2} \tag{5}$$

If the driving signal is not sinusoidal, Fourier component at various frequencies should also be taken into consideration. FoM provides a way to compare the performance of various DFLC mixtures at different operating conditions. It also provides useful guidelines in material development to achieve fast response time. Increasing birefringence effectively boosts the FoM and thereby decreases the response time. Low rotational viscosity is always desirable. Large dielectric anisotropy helps to reduce the threshold voltage and therefore is favorable.

3.2.3 High birefringence DFLC using 3-ring NCS tolane compounds

High Δn DFLC materials are equally favoured from fast response time and low operating voltage viewpoints. Positive Δε compounds in most DFLC mixtures contain at least one ester linking group, which contribute to the dielectric relaxation. The ester linking group helps to lower the crossover frequency, but it breaks the π-electron conjugation [Fig. 1(a)]. Therefore, the birefringence of such compounds is limited. Commercial DFLC mixtures hardly exhibit a birefringence higher than 0.2. Since elongating the π-electron conjugation of LC compounds is the most effective way to increase birefringence, we introduce new positive $\Delta\varepsilon$ compounds with a highly conjugated π-electron core structure into DFLC mixtures. The tolane linking group of the new compounds contributes to π-electron conjugation. We have designed and synthesized 3-ring NCS tolane compounds with a structure shown in Fig.1 (b). In the structure, lateral difluoro on the middle ring of the compounds provides an effective dipole moment perpendicular to the principal axis, contributing to a negative Δε at high frequencies. Total dipole moment of the single fluoro and the NCS terminal group is approximately parallel to the principal molecular axis, which will contribute to a positive Δε at low frequencies. The long rigid core structure of these compounds helps to lower the crossover frequency. Such a unique structure allows these compounds to replace the ester-based positive compounds in DFLC mixtures. Since NCS phenyl-tolane molecules are linearly conjugated, they exhibit a significantly higher birefringence than the comparative esters.

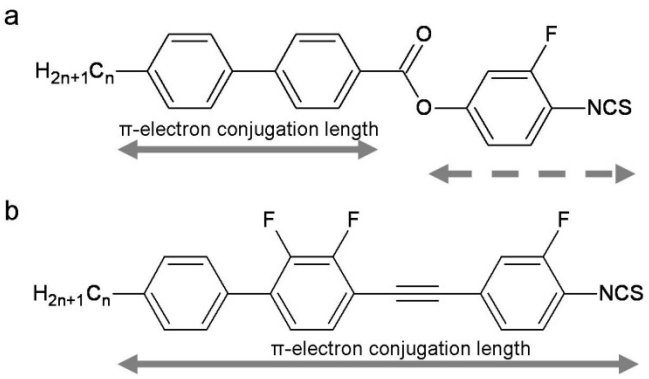

Fig.1. (a) Molecular structure of a traditional ester positive Δε compound, and b) Structure of a new highly conjugated positive Δε compound.

Based on these high performance new positive compounds, we formulated a record-high birefringence DFLC mixture (new UCF-DFLC) by mixing 60% NCS tolanes with 40% laterally fluorinated tolane negative compounds. Figure 2(a) shows the frequency dependent Δε of this new UCF-DFLC at various temperatures. Table 1 shows the fitted dielectric relaxation properties for this DFLC mixture in comparison with the commercial DFLC mixture Merck MLC-2048 at 25˚C. New UCF-DFLC shows a $\Delta\varepsilon$ of 3.8 at low frequency limit and -4 under high frequency limit, larger than that of MLC-2048. Large dielectric anisotropy is preferred for fast response time. The crossover frequencies (f_c) for the two DFLC mixtures are plotted against temperature in Fig. 2(b). The activation energy for new UCF-DFLC and MLC-2048 is 625.7 meV and 723.2 meV, respectively. From this figure, we found that new UCF-DFLC shows a slightly lower crossover frequency than MLC-2048.

Table 1. Dielectric relaxation properties of new UCF-DFLC and MLC-2048 at 25˚C.

	$\Delta\varepsilon(0)$	$\Delta\varepsilon(\infty)$	f_c (kHz)	E (meV)
new UCF-DFLC	3.8	-4	26.8	625.7
MLC-2048	2.82	-3.24	31.7	723.2

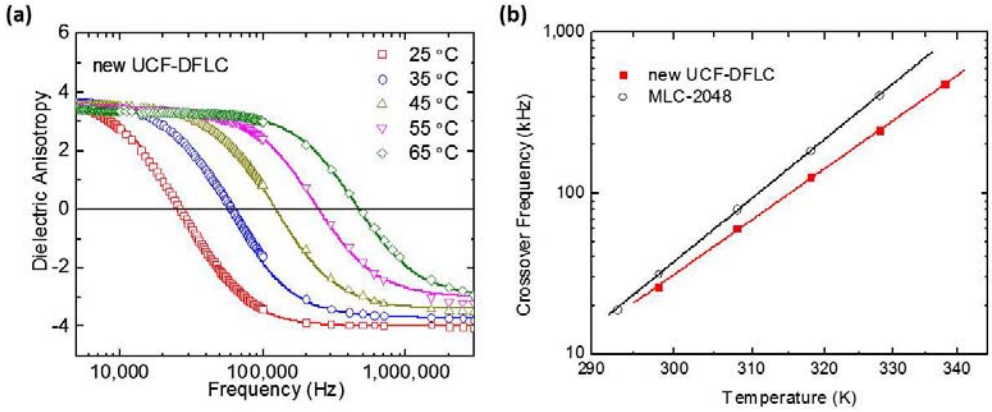

Fig. 2 (a) Frequency dependent dielectric anisotropy under different temperatures for new UCF-DFLC; b) The plot of the crossover frequency versus temperature for new UCF-DFLC and MLC-2048.

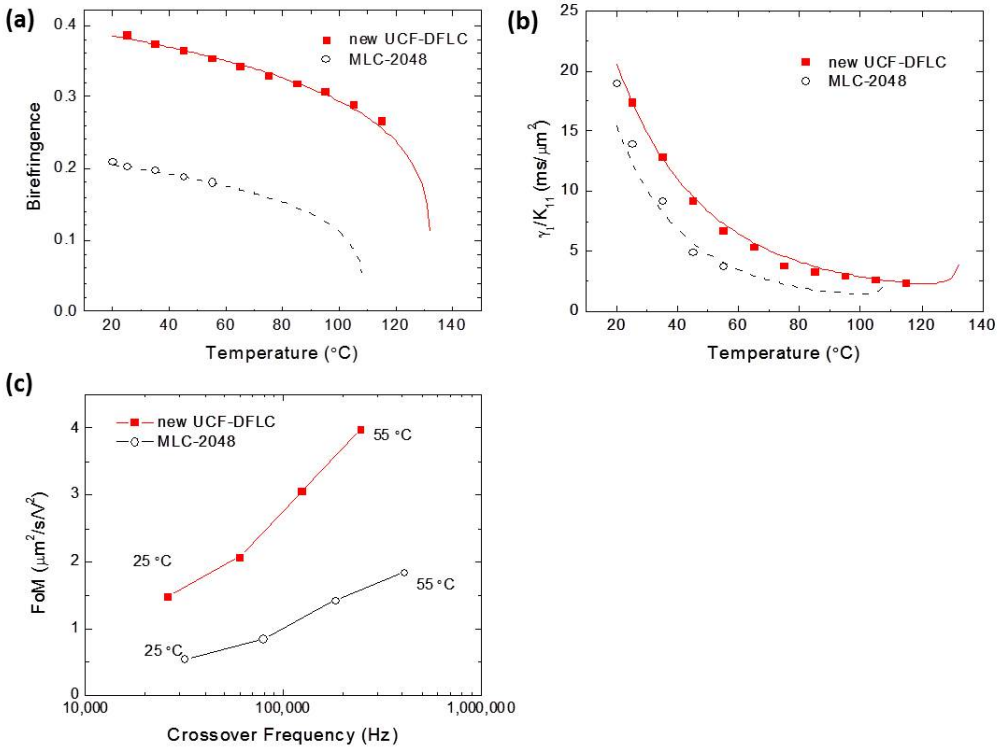

Fig. 3 Temperature dependent electro-optical properties of new UCF-DFLC and MLC-2048.

The temperature dependent birefringence and visco-elastic coefficient of the new UCF-DFLC and MLC-2048 is presented in Figs. 3(a) and 3(b), respectively, together with the fitting results. With no surprise, new UCF-DFLC exhibits a much higher birefringence. Its Δn=0.38 at 25˚C (λ=633 nm), which is significantly higher than the birefringence of MLC-2048 (Δn=0.202). This is the highest birefringence ever reported in DFLC mixtures. From Fig. 3(b), we found the visco-elastic coefficient of new UCF-DFLC is slightly higher than that of MLC-2048. The calculated FoM for the two DFLC Mixtures is plotted against the crossover frequency in Fig.3(c). Our UCF-DFLC exhibits much higher FoM than MLC-2048.

3.2.4 UCF-01: ultralow crossover frequency DFLC using four ring single ester cyanato compounds

All the physical properties of a thermotropic LC are temperature dependent. Birefringence, viscosity, and dielectric anisotropy all decrease as the temperature increases but at different rates. The combined effect is that the temperature dependence of FoM_{DFLC} has the following form:

$$FoM_{DFLC} \propto \left(1-\frac{T}{T_C}\right)^{2\beta} \cdot \frac{1}{kT} \exp\left(-\frac{E}{kT}\right) \tag{6}$$

From Eq. (6), as the temperature increases, viscosity decreases at a faster rate than birefringence and dielectric anisotropy. Thus, *FoM* increases with the operating temperature, reaches a peak, and then declines sharply as the operating temperature gets closer to the clearing point. This tendency also holds for ordinary nematic LCs when the device is operated at an elevated temperature for improving response time. In the case of DFLC, however, the temperature dependence of crossover frequency sets a strong limit to the operating temperature. The crossover frequency of DFLC increases exponentially with the operating temperature. The high frequency used for restoring the LC directors cannot be too high from the viewpoints of power consumption, induced heating effect at electrodes, and dielectric heating effect of DFLC material itself. Therefore, to take advantages of elevated temperature operation of a DFLC device, a delicate balance between substantially reduced viscosity and exponentially increased crossover frequency should be taken into consideration simultaneously.

We have developed a DFLC mixture, UCF-01, with ultralow crossover frequency using four ring single ester compounds and laterally difluoro tolanes and phenyl tolanes. The crossover frequency of this mixture is below 1 kHz at 25 °C. Such a low crossover frequency enables the DFLC device to be operated at an elevated temperature in order to substantially reduce the rotational viscosity and boost the *FoM*. Table 2 lists the temperature dependent electro-optic properties of UCF-01. Also included for comparisons are DFLC-2 (a UCF DFLC optimized for room temperature operation), and Merck MLC-2048. From Table 2, although the crossover frequency of UCF-01 also increases with the temperature, it is only 5.8 kHz at 45 °C and 13.5 kHz at 55 °C. If we choose 90% decrease in $\Delta\varepsilon$ as the criterion for high operating frequency, the crossover frequency should be limited to 1/3 of the high driving frequency. That is, if we choose 30 kHz as the high driving frequency, then the crossover frequency of the DFLC should be lower than 10 kHz so that most of the negative $\Delta\varepsilon$ at high frequency region can be utilized.

Table 2. Electro-optical properties of UCF-01 at various temperatures, and the electro-optical properties of DFLC-2 and MLC-2048 at operating temperatures.

	UCF-01				DFLC-2	MLC-2048
	25 °C	35 °C	45 °C	55 °C	22 °C	20 °C
Δn (λ=1550 nm)	0.248	0.247	0.246	0.239	0.247	0.189
γ_1/K_{11}	35	21	15	8.4	28	20
V_{th} (V)		1.85	1.82	1.86	2.03	2.39
FoM_{DFLC} (low frequency)		0.84	1.24	1.96	0.52	0.31
FoM_{DFLC} (high frequency)		0.54	0.80	1.25	0.40	0.36
Crossover Freq. (kHz)	0.8	2.3	5.8	13.5	10	18.9
Δε (0)	6.6	6.1	5.7	5.3	6.2	2.9
Δε (∞)	-4.1	-3.9	-3.7	-3.4	-4.8	-3.3

We chose 30 kHz as the high frequency for erasing the UCF-01 cell. If we slightly relax the restriction in crossover frequency, UCF-01 can still be operated at 55 °C where the crossover frequency is 13.5 kHz. The crossover frequency of DFLC-2 is 10 kHz at 22 °C. Therefore, the DFLC-2 phase retarder was operated at 22 °C. The crossover frequency of MLC-2048 is already 19 kHz at 20 °C, thus, a 30 kHz high operating frequency is

insufficient. In order to operate the MLC-2048 phase retarder at 20 °C, we increased the high driving frequency to 50 kHz. Figure 4 depicts the FoM_{DFLC} (low frequency) vs. crossover frequency of UCF-01, DFLC-2, and MLC-2048. The limit of operating temperature and achievable FoM_{DFLC} casted by the crossover frequency is indicated in this figure.

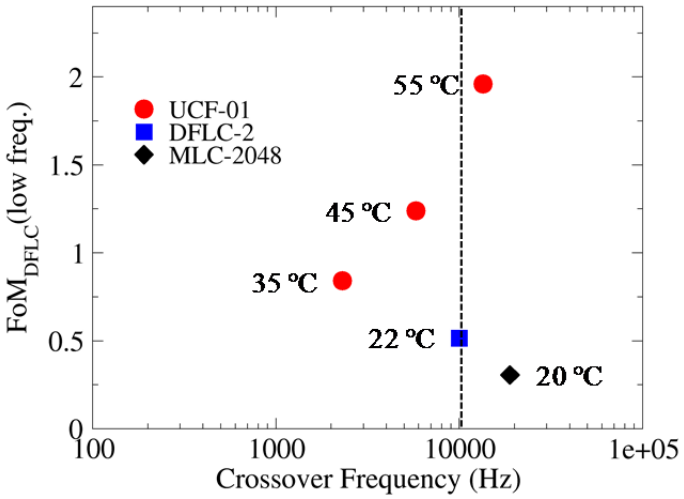

Fig. 4 The FoM_{DFLC} at low frequency region vs. crossover frequency of UCF-01, DFLC-2, and MLC-2048.

Then we used UCF-01 to demonstrate a high speed phase retarder with 2π phase change at λ=1.55 μm. The DFLC mixture was capillary-filled into an ITO (indium tin oxide) coated glass cell with antiparallel rubbed polyimide alignment layers. The cell gap is 10.24 μm and the total phase retardation is more than 3π at 1.55 μm. The redundancy in cell gap is to prevent electro-hydrodynamic instability at a high operating voltage. The phase retarder was placed between two crossed polarizers with its optic axis oriented at 45° with respect to the transmission axis of the polarizer. The transmittance of the system was measured and converted to phase retardation. A 500 Hz square-wave driving signal was applied to hold the device at the on and off states. The response time of the phase retarder with a 2π phase change was measured at 35 °C, 45 °C, and 55 °C. For comparison, we also measured the response time of the DFLC-2 and MLC-2048 cells. The cell gap for the DFLC-2 phase retarder was 10.16 μm, and for the MLC-2048 one was 13.37 μm. The cell gaps of the retarders were so chosen that the total phase retardation is close to that of the UCF-01 retarder. The measured response time at all three temperatures are listed in Table 3. At 55 °C, τ_{on+off} ~ 754 μs. Thus, a submillisecond response modulator with 2π phase change at 1.55 μm was achieved. For a shorter wavelength, the required cell gap can be reduced accordingly which in turn leads to a shortened response time. As the temperature increases, the response time of the phase retarder decreases substantially. This can be directly correlated to the temperature dependence of FoM_{DFLC} shown in Table 3. Figure 5 depicts the response time vs. $1/FoM_{DFLC}$ for UCF-01 at different operating temperatures. We derived the FoM_{DFLC} such that with the same phase retardation, the response time is proportional to $1/FoM_{DFLC}$. This is supported by the data of UCF-01 in Fig.5. To further validate this correlation, the FoM_{DFLC} and response time of DFLC-2 and MLC-2048 phase retarders were also measured and results included in Fig. 5. These data agree well with our expectation.

Table 3 FoM_{DFLC} and turn-on/off times of the phase retarders.

	UCF-01			DFLC-2	MLC-2048
	35 °C	45 °C	55 °C	22 °C	20 °C
FoM_{DFLC} (low freq.)	0.84	1.24	1.96	0.52	0.31
τ_{on} (μs)	890	552	304	1110	1660
FoM_{DFLC} (high freq.)	0.54	0.80	1.25	0.40	0.36
τ_{off} (μs)	803	589	450	1240	1340

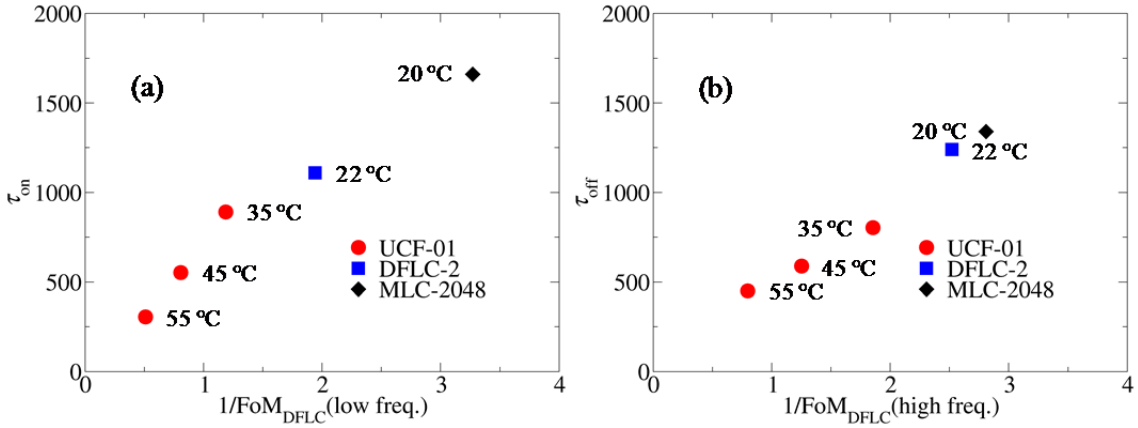

Fig. 5 Measured response time vs. $1/FoM_{DFLC}$ for (a) turn-on and (b) turn-off processes of three DFLC phase retarders. λ=1550 nm.

3.2.5 UCF-02: A high birefringence and ultra-low crossover frequency DFLC

In Section **3.2.4**, we have demonstrated an ultra-low crossover frequency DFLC UCF-01 using four ring single ester cyanato compounds. The long rigid core bestows low relaxation frequency to these compounds. However, the ester linking group limits the birefringence of these compounds. Later we find that replacing ester with carbon-carbon triple bond indeed elongates the π electron conjugation length while maintaining a low relaxation frequency. Based on this finding, we replaced the ester group in the core structure of the four ring single ester cyanato compounds with the conjugating carbon-carbon triple bond and derived several high birefringence ultra-low relaxation frequency compounds for DFLC. We characterized the physical properties of these compounds and the results validated our design concepts. Table 4 depicts the molecular structures of investigated high birefringence ultra-low relaxation frequency positive compounds. In our notations, P stands for phenyl ring, C for cyclohexane ring, T for carbon-carbon triple bond, CN for cyanato functional group, (3,5F) for fluoro substitutions at the 3 and 5 position of the phenyl ring. The number before CN is the alkyl chain length on the other end of the molecule. The long conjugated rigid core structure bestows these compounds a high birefringence (0.3~0.4) and ultra-low Debye relaxation frequency. Table 5 lists the dielectric relaxation properties of two new compounds CPTPP(35F)5CN and PPTPP(3,5F)-3/5CN at a series of temperatures

Table 4 Molecular structure and mesomorphic properties of the high birefringence ultra-low relaxation frequency compounds.

	Structure	Tm (°C)	Tc (°C)	ΔH (cal/mol)
CPTPP(3,5F)-3CN	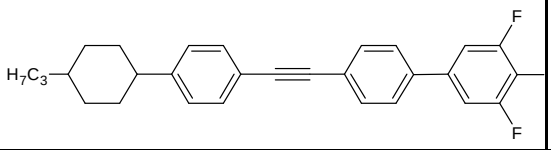	136	343	5121
CPTPP(3,5F)-5CN	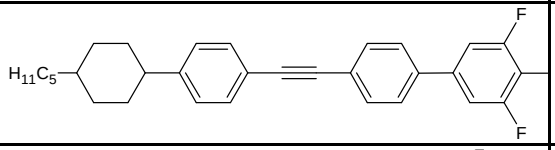	125	330	4971
PPTPP(3,5F)-3CN	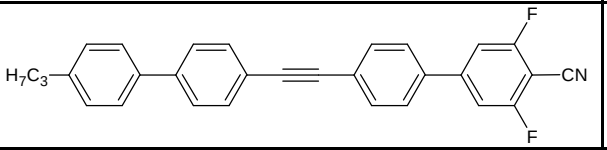	224	346	7054
PPTPP(3,5F)-5CN	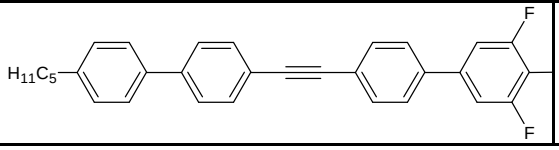	183	331	6697

Table 5 Dielectric relaxation properties of CPTPP(35F)5CN and PPTPP(3,5F)-3/5CN various temperatures.

CPTPP(35F)5CN	25 °C	35 °C	45 °C	55 °C	65 °C
$\Delta\varepsilon(0)$	29.3	27.2	24.9	23.2	21.3
$\Delta\varepsilon(\infty)$	-3.4	-3.6	-3.9	-4.4	-4.8
f_r (kHz)	2.0	5.8	15.8	39.5	92.3

PPTPP(3,5F)-3/5CN	25 °C	35 °C	45 °C	55 °C	65 °C
$\Delta\varepsilon(0)$	37.4	36.5	34.2	31.8	29.2
$\Delta\varepsilon(\infty)$	0.8	0.8	0.5	-0.1	-0.7
f_r (kHz)	1.8	5.0	13.4	34.5	81.8

Using these compounds, we have formulated a new DFLC mixture with high birefringence and ultra-low crossover frequency, designated as UCF-02, for elevated temperature operation. The composition of the mixture was listed in Table 6. Tolane and phenyl-tolane compounds with negative $\Delta\varepsilon$ were adopted because of their high birefringence. Due to their high melting temperature and large heat fusion enthalpy, the concentration of PPTPP(3,5F)-3CN and PPTPP(3,5F)-5CN is rather limited.

Table 6 Compositions of the high Δn ultra-low crossover frequency DFLC mixture UCF-02.

	Molecular Structure	
Tolane	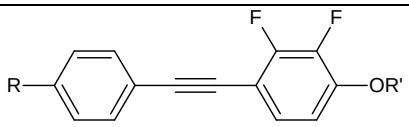	12%
Cyclohexane Tolane	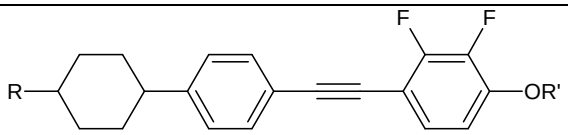	25%
Phenyl Tolane	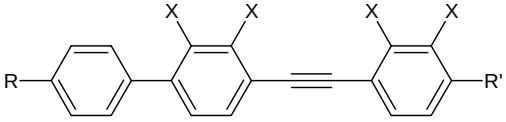 R, R': alky or alkoxy end groups; X: at least 2 neighboring X on a phenyl ring are fluorine, others are hydrogen.	40%
PP(23F)5-O2	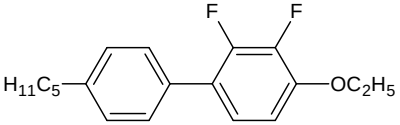	5%
C/PPTPP(35F)xCN	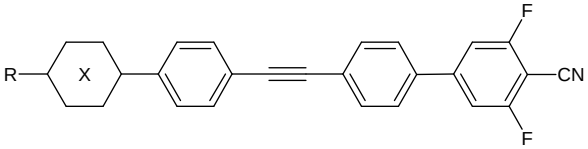 R: C_3H_7 or C_5H_{11};  : phenyl or cyclohexane	20%

The dielectric relaxation and electro-optical properties of UCF-02 were characterized at elevated temperatures, and the results are listed in Table 7. As expected, the crossover frequency of UCF-02 is only 1.2 kHz at 25°C, and remains less than 10 kHz at 45 °C. This makes UCF-02 ideally suitable for operation at elevated temperatures for achieving fast response time. In comparison, the crossover frequency of Merck MLC-2048 at 20°C is already 18.9 kHz. As the temperature increases, its crossover frequency increases exponentially, making it difficult to operate at elevated temperatures. Table 7 also includes the birefringence at λ=633 nm, visco-elastic constant, and FoM of UCF-02 at elevated temperatures. For comparison, the properties of Merck MLC-2048 at 20°C are also included there. The birefringence of UCF-02 is higher than 0.3 at 25°C and wavelength λ=633 nm.

Table 7 Dielectric relaxation and electro-optical properties of UCF-02.

	UCF-02				MLC2048
T (°C)	25	35	45	55	20
Δn	0.305	0.299	0.295	0.294	0.210
γ_1/K_{11} (ms/μm^2)	27.2	16.8	11.1	8.8	18.97
FoM_{DFLC} (μm^2/sV^2)	0.63	1.06	1.55	2.11	0.385
Δε (0)	4.98	4.51	4.21	4.22	2.87
Δε (∞)	-3.12	-2.92	-2.76	-2.57	-3.35
f_c (kHz)	1.2	3.2	7.7	17.0	18.9

Figure 6 shows the FoM of UCF-02 vs. crossover frequency at the four specified temperatures. UCF-02 exhibits a lower crossover frequency at 55°C than that of MLC-2048 at 20°C. As we mention earlier, the maximum achievable *FoM* is limited by the crossover frequency. From Fig. 6, under the same crossover frequency limitation, the figure of merit of UCF-02 is 5X higher than that of MLC-2048, and UCF-02 can achieve more than 5X faster response time than MLC-2048.

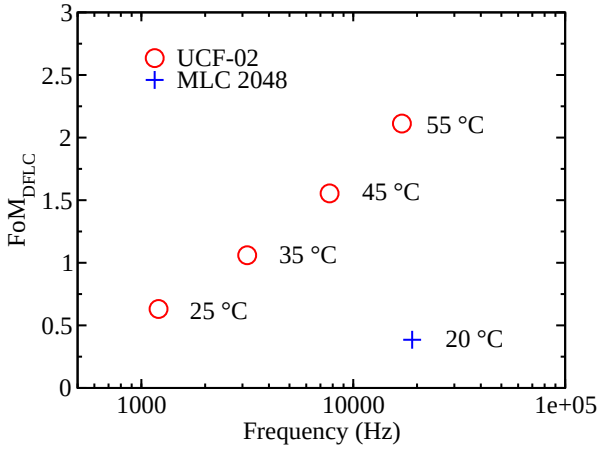

Fig. 6 Figure of Merit (FoM) vs. crossover frequency of UCF-02 and MLC-2048

3.2.5 Summary

We have developed a series of DFLC mixtures with high birefringence and ultra-low crossover frequency. Merck DFLC mixture MLC-2048 is listed as a benchmark, its Δn =0.202 at λ=633 nm and 25 °C, crossover frequency ~18.9 kHz at 20 °C.

UCF-DFLC: record-high birefringence DFLC mixture, Δn=0.38 at λ=633 nm and 0.33 at λ=1550 nm at 25 °C.

UCF-01: It is an ultra-low crossover frequency DFLC mixture designed for elevated temperature operation. Its crossover frequency is only 5.8 kHz at 45 °C and 13.5 kHz at 55 °C. Using UCF-01, we demonstrated a DFLC

phase modulator with a 2π phase change at λ=1.55 μm, submillisecond (τ_{on} +τ_{off} <0.8 ms) response time, and merely 40 V_{rms} operation voltage at 55°C.

UCF-02: Δn=0.305 at λ=633nm, 25°C, the crossover frequency at room temperature is only 1.2 kHz and increases slowly to 17 kHz at 55°C. Under the same crossover frequency limitation, the figure of merit of UCF-02 is 5X higher than that of MLC-2048 and UCF-02 can achieve more than 5X faster response time than MLC-2048.

3.3 Submillisecond-response and Scattering-free Polymer Network Liquid Crystals (PNLC)

3.3.1 Introduction

Fast-response LC devices with a large phase change (≥2π) are highly desirable for photonic applications, such as laser beam steering and adaptive lens. However, to achieve a large phase shift would require a fairly thick LC layer, which dramatically increases the response time. This problem gets worse in infrared region due to longer wavelength and lower birefringence. PNLC is an effective way to achieve both fast response and large phase change. However, light scattering takes place in the voltage-on state at near infrared wavelength region (λ=1.06 μm, 1.55 μm) because LC domain sizes are larger than the wavelength. A common way to suppress scattering is to reduce domain sizes by increasing polymer concentration. The tradeoff is the largely increased operating voltage. Non-mesogenic monomers have to be used in such PNLCs, which reduces operating voltage but also disturbs the LC alignment. A typical response time for 2π phase change at λ=1.06 μm or 1.55 μm of such a PNLC is around 1 ms at room temperature.

In order to shrink domain sizes and eliminate scattering for a PNLC device, several factors should be taken into consideration, such as monomer, LC host, UV intensity, photo-initiator concentration. In our study, we concentrate on the monomer and LC host effects.

3.3.2 Monomer effect on PNLC

Monomer plays an essential role in determining the PNLC domain sizes and operating voltage. A typical LC gel (scattering mode PNLC) contains 6-8 wt% di-functional monomer. Figure 7 lists some examples of di-functional monomers used in PNLC. As the monomer ratio increases, LC domain size decreases, leading to reduced scattering loss but increased operating voltage.

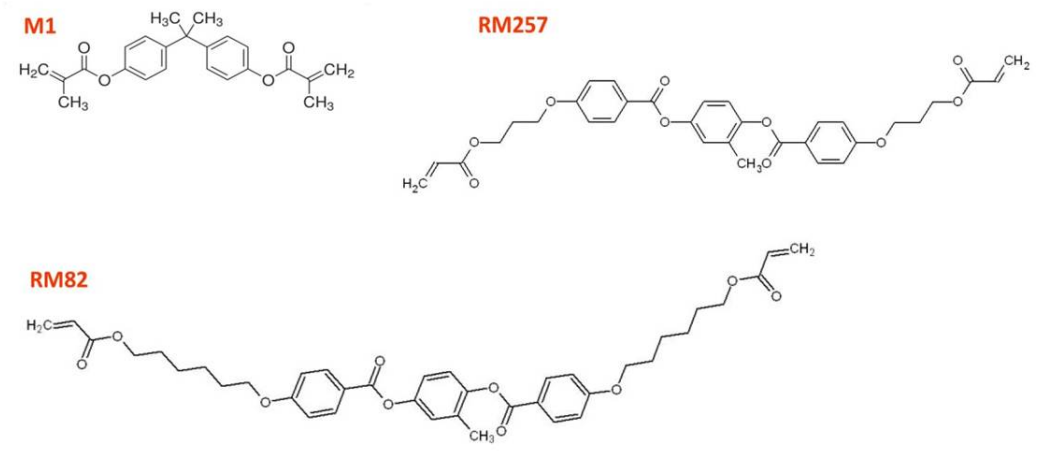

Fig.7 Examples of di-functional monomers used in PNLC.

By increasing the monomer ratio to 10%, a scattering-free PNLC (PNLC-A) was developed at λ=1.55 μm. The cell gap of PNLC-A is 12 μm. However, if we operate PNLC-A at λ=1.06 μm its scattering loss exceeds 20% because the scattering loss is strongly wavelength dependent. To suppress scattering, we increased the monomer ratio to 12% (PNLC-B). Figure 8 depicts the measured voltage-dependent transmittance (VT) curves of PNLC-A and PNLC-B at 1.06 μm. Note that the peak transmittance of PNLC-B is comparable to that of a 12-μm nematic LC host cell, which means PNLC-B is free from scattering at λ=1.06 μm. Due to the strong anchoring effect of polymer network and large elastic constant, both PNLCs exhibit submillisecond response time.

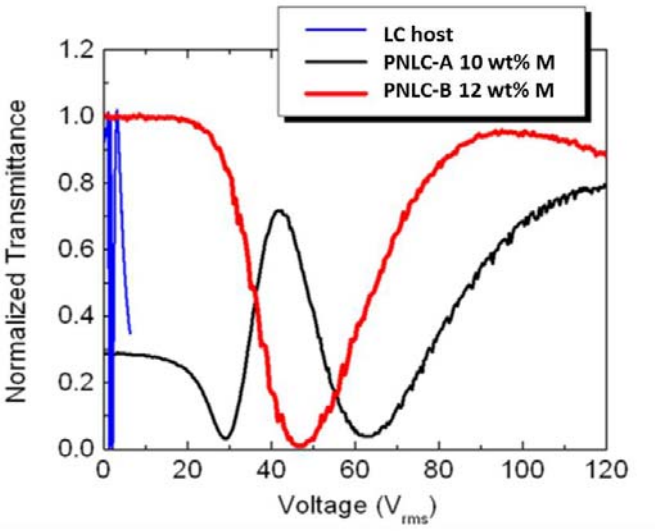

Fig. 8 Measured VT curves of PNLC-A and PNLC-B at λ=1.06 μm.

In PNLC-A and PNLC-B, we used a non-mesogenic monomer (M1, Fig. 7) to help reduce voltage. Although M1 helps lower the operating voltage, it disturbs the LC alignment. As a result, it causes nonuniform phase profile spatially, which is problematic for a spatial light modulator (SLM). Figure 9 shows the photographs of two PNLC samples sandwiched between two crossed polarizers on a white light table. The left one containing both non-mesogenic monomer M1 and mesogenic monomer RM257 exhibits nonuniform color distribution due to the poor LC alignment while the right one (RM257 only) shows a uniform color. The problem is if we use 10-12% RM257 in a PNLC, the operating voltage would be quite high because M1 helps to create a large pretilt angle, which in turn weakens the anchoring force between polymer network and LC molecules. Therefore, new strategy is needed in order to use a minimal amount of polymer for reducing operation voltage while keeping stable networks and negligible scattering.

Fig. 9 Photographs of two PNLCs containing different types of monomers.

3.3.3 Viscosity effect on PNLC

In a PNLC, nematic host occupies ~90% by weight, which plays the key role to determine the final performance. Meanwhile, the domain sizes also highly depend on the employed nematic LC host. To verify this, we prepared a series of PNLC samples based on five different nematic hosts. We first mixed LC host with 6 wt% Merck RM257 monomer and 0.5 wt% photoinitiator Irgacure 819. The prepared mixture was then filled into an empty homogeneous LC cell whose pretilt angle is ~3°. Cell gap *d* was 12 μm, ensured by spacer rods. An ultraviolet light source (λ=385 nm and intensity ~200 mW/cm^2) was used to illuminate the sample cell for one hour. The curing temperature for PNLC 1-5 was 22℃ (room temperature). Table 8 lists the physical properties of the five LC hosts for making PNLC 1-5 at 22℃.

Table 8 Physical Properties of the Five LC Hosts Used in PNLC 1-5 (22 °C).

PNLC	LC host	γ_1/K_{11} (ms/μm^2)	γ_1 (Pa·s)	K_{11}(pN)	Δε (1kHz)	Δn@1.06μm
1	MLC14200 (Merck)	27.3	0.27	9.9	25	0.15
2	E44 (Merck)	27.3	0.33	12.1	16	0.22
3	BL038 (Merck)	40.7	0.56	13.8	16	0.23
4	HTG135200 (HCCH)	119.6	1.20	10.0	86	0.19
5	BP1 (HCCH)	153	1.52	9.9	50	0.15

To analyze the scattering loss of PNLC, we proposed a Rayleigh-Gans-Debye model of scattering. This approximation is valid when the domain size is comparable to the wavelength while the phase shift caused by the scattering domains is small: $D\delta n_{eff} << 2\pi\lambda_m$. Here, D is the average domain size, δn_{eff} is the effective refractive index difference, and $\lambda_m=\lambda_0/n$ is the wavelength in the medium. Considering scattering of PNLC is highly polarization dependent, o-ray (polarization perpendicular to rubbing direction) and e-ray (polarization parallel to rubbing direction) have different extinction ratio α, the transmittance of PNLC for a randomly polarized light at V_{max} (where maximum scattering occurs) can be written as:

$$T = \frac{1}{2}\exp\left(-C_e \frac{\Delta n^2}{\lambda_0^2} d\right) + \frac{1}{2}\exp\left(-C_o \frac{\Delta n^2}{\lambda_0^2} d\right), \tag{7}$$

where C_e and C_o represent the domain size parameters for e-ray and o-ray, respectively.

Figure 10 shows the measured transmission spectra of PNLC 1-5 with V_{max} applied (solid lines). Data points between 780 nm and 1000 nm are missing because the spectrometer detectors have very low sensitivity in this region. A 12-μm cell filled with BK7 matching liquid was used for normalization purpose. Sample holder was set at 20 cm in front of a photodiode detector with an aperture of 0.9 cm, corresponding to a collection angle ~2.6°. Such a small collection angle ensured that light scattered by LC multi-domains was not collected by the detector. The oscillations in spectra are caused by Fabry-Perot effect, since the refractive index mismatch between indium tin oxide and liquid/liquid crystals increases as the wavelength goes up. Domain size parameters are plotted against the reciprocal of rotational viscosity (γ_1) of LC hosts in Fig. 11(a). To confirm the fitting results, we measured the transmission spectra for o-ray and e-ray and fitted independently from λ=500 nm to λ=700 nm (spectra not shown). The extracted domain size parameters (C_{ep}, C_{op}) are plotted in Fig. 11(a), in good agreement with those extracted from Fig. 10. As expected, C_o (or C_{op}) is negligible as compared to C_e (or C_{ep}), because ideally there shouldn't be voltage-induced phase change for the o-ray. A linear relationship is found between domain size parameters and γ_1^{-1}, which can be explained by Stokes-Einstein theory. The mean square displacement of a particle suspended in a liquid is described as:

$$\overline{x^2} = \frac{k_B T}{3\pi\eta R} t, \tag{8}$$

where k_B is the Boltzmann constant, T is the Kelvin temperature, η is the flow viscosity, R is the radius of the particle and t is the time interval. Under the same reaction rate, monomers show shorter coherence length in a more viscous LC host. Instead of aggregating into thick fibrils, monomers tend to form finer polymer networks. Since the rotational viscosity γ_1 generally has a linear relationship with flow viscosity η, the domain size parameter is proportional *to* γ_1^{-1}.

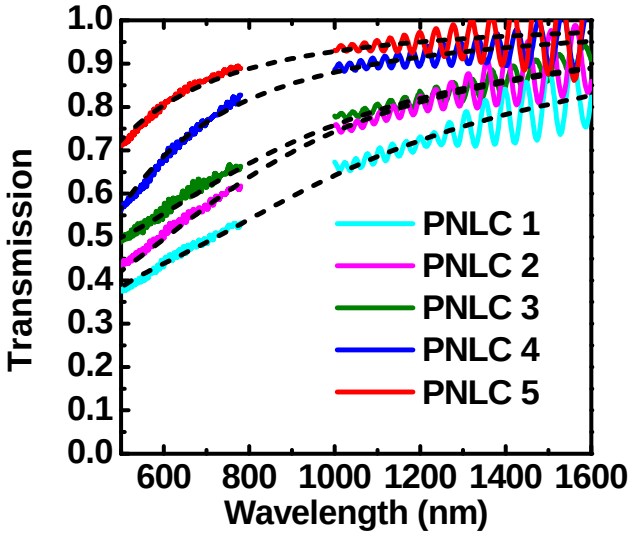

Fig. 10 Transmission spectra of PNLC 1-5 with V_{max} applied. Solid lines: experimental results; dashed lines: fitting results with Eq. (7).

Under small angle approximation, the LC director's relaxation time of a homogeneous cell can be approximated as $\tau \sim \gamma_1 d^2/K_{11}\pi^2$; where d is the LC cell gap, γ_1 is the rotational viscosity and K_{11} is the splay elastic constant. As viscosity increases, LC response time increases. However, for PNLCs, the characteristic lengths are much shorter than the cell gap d, because the polymer network divides the LC cell into multiple nano/micro-domains. Thus, the cell gap d can be replaced with the average domain size D. Since D is proportional to γ_1^{-1} according to our study, τ is supposedly proportional to $(\gamma_1 K_{11})^{-1}$. From this prediction, a higher viscosity LC host tends to produce a PNLC with faster response time (because of smaller domain sizes). In contrast, a nematic LC prefers low viscosity to achieve fast response.

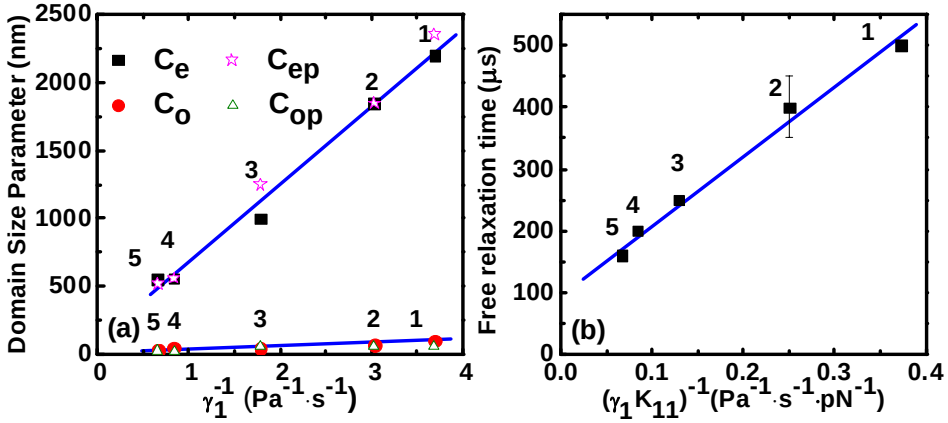

Fig. 11. (a) Plot of domain size parameters of PNLC 1-5 versus γ_1^{-1} of the corresponding LC hosts. (b) Plot of free relaxation time constant of PNLC 1-5 versus $(\gamma_1 K_{11})^{-1}$. Straight lines are for visual guide only.

To validate this prediction, we measured the relaxation time of PNLC 1-5. Figure 11(b) depicts the free relaxation time τ of PNLCs versus $(\gamma_1 K_{11})^{-1}$ for the corresponding LC hosts. We find that PNLC-5 based on the most viscous LC host shows the fastest response time while PNLC-1 with the least viscous LC is the slowest. Response time generally follows the linear relationship with $(\gamma_1 K_{11})^{-1}$ as predicted.

3.3.4 A 2π phase modulator at λ=1.06 μm

To fabricate a 2π phase modulator at λ=1.06 μm while eliminating light scattering, we need to choose a proper LC host. Note that the average domain sizes for PNLC-4 and PNLC-5 are quite close, but PNLC-5 shows less scattering mainly because of its lower birefringence. However, a smaller Δn would require a thicker cell gap in order to obtain

2π phase change. Since No.4 LC host (HTG 135200) has a larger Δε which is helpful for reducing operating voltage, we consider it as the best choice among these five LC hosts. PNLC-6 was prepared with the same precursor as PNLC-4, but cured at 11°C. From the modified Arrhenius model, rotational viscosity of nematic LC can be described by $\gamma_1 = b \cdot S \cdot exp(E_a/k_BT)$, where b is a proportionality constant, E_a is the activation energy, S is the order parameter, and K_B is the Boltzmann constant. As the temperature is reduced from 22°C to 11°C, the viscosity of LC host 4 increases from 1.2 Pas to 2.1 Pas. Thus, the prepared PNLC is expected to have smaller domain sizes. Figure 12(a) depicts the measured transmission spectrum of PNLC-6 with a bias voltage $V_{max}=50V_{rms}$ (red solid lines). At λ=1.06μm the transmittance exceeds 97% (c.f. the transmittance of PNLC-4 is <90% as Fig. 10 shows), indicating that PNLC-6 has a smaller average domain size than PNLC-4. The free relaxation time of PNLC-6 is 110 μs and PNLC-4 is τ=200 μs at the room temperature. This also indicates that PNLC-6 has smaller average domain size than PNLC-4.

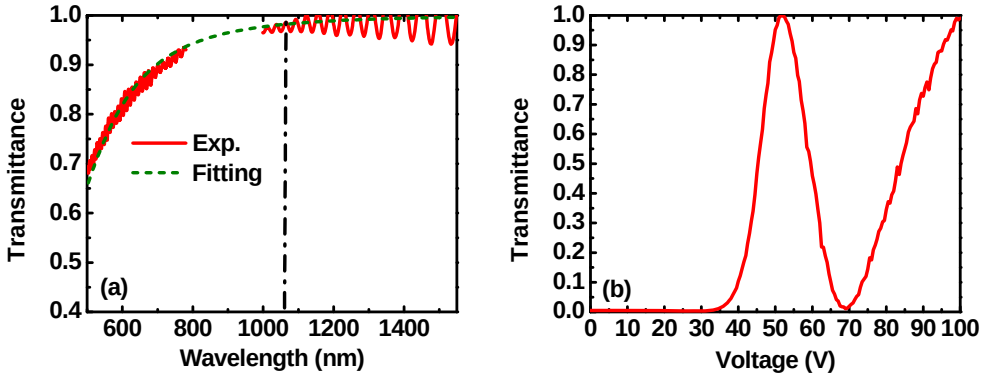

Fig. 12 (a) On-state light transmission spectra of PNLC-6 at $V_{max}=50V_{rms}$ (the voltage leading to maximum scattering loss). The vertical dashed lines indicate λ=1064 nm. (b) Measured voltage dependent transmittance curve of PNLC-6 at 25°C and λ=1064 nm.

Figure 12(b) depicts the measured voltage dependent transmittance of PNLC-6 between two crossed polarizers for λ=1.06μm. Driving frequency is 5 kHz. As the applied voltage increases from 0 to 100V, the total phase shift is 3π. The required voltage for 2π phase change is ~70 V. Figure 13 shows the temperature dependent response time of PNLC-6 for a 2π phase shift, which is defined as the time interval for phase changes from 100% to 10%. At 25 °C, the measured rise time is 207 μs and decay time is 220 μs. As the temperature increases to 70 °C, the measured decay time is decreased to 30 μs while rise time is decreased to 28 μs because of the reduced viscosity. However, the operating voltage increases to 90V mainly because of the decreased birefringence. As most polymer-stabilized LC systems have hysteresis issues, our PNLC-6 shows a 7.7% hysteresis at 25°C and 2% hysteresis at 70°C.

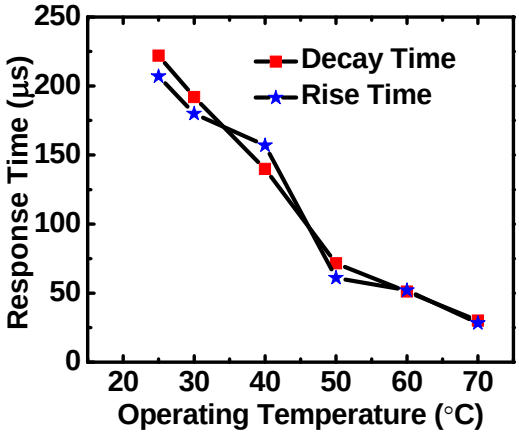

Fig. 13 Temperature dependent 2π phase change response time for PNLC-6 at λ=1.06 μm.

3.3.5 Summary

Through our study on the viscosity effect of liquid crystal hosts on PNLCs, we find that that the domain size is inversely proportional to the viscosity of the LC host. The free relaxation time constant τ is found to be proportional to $(\Upsilon_1 K_{11})^{-1}$. Also, samples based on viscous LC host exhibit faster response time compared to those adopting less viscous nematic host. This is completely opposite to what we know for nematic LCs which favors low viscosity for fast response time. Based on this discovery, with selected high viscosity LC host and only 6 wt% reactive mesogen monomer, we demonstrated a nearly scattering-free (<3%) 2π phase modulator at λ=1.06 μm. The operating voltage is ~70V at room temperature. The relaxation time for 2π phase shift is 220 μs at 25°C and 30 μs at 70°C. Comparing with previous PNLC phase modulator, the improvement on relaxation time is ~4X. In contrast, the 2π relaxation time of traditional E7 nematic LC phase modulator (d=12 μm) is ~200 ms (25 °C). This ~1000X improvement in response time is attributed to the thinner effective LC thickness. If reflective mode is employed, we could lower the operating voltage by ~30% for the same amount of phase modulation. To further eliminate scattering, we can slightly increase the polymer ratio. Using a large dielectric anisotropy LC host is helpful to compensate the increased operating voltage.

3.4 Low Absorption Liquid Crystals for MWIR Applications

3.4.1 Introduction

Linearly conjugated LCs exhibit a relatively high birefringence in the IR region and thus have been used in the 8-12 μm range as dynamic scene projectors for IR seekers, and at λ=10.6 μm and 1.55 μm for laser beam steering and IR light shutters, and photonic crystal fibers. A major concern for IR applications using LCs is the inherent absorption loss due to the existence of molecular vibration bands. Even in off-resonance regions, the baseline absorption coefficient may reach as high as α~10 cm^{-1}, but if the LC layer is thin (~5 μm) then the absorption loss may still be negligible. However, to achieve a sufficient phase change a minimum cell gap is required. As the cell gap increases, the absorption loss increases exponentially. In the vicinity of resonance wavelengths where α could reach 10^4 cm^{-1}, then a 5-μm LC layer is now essentially opaque.

In the MWIR region (3-5 μm), several molecular vibration bands exist, such as CH, CH_2, CH_3, CN, and NCS stretching. The CH, CH_2, and CH_3 absorption bands overlap closely and are centered at ~3.4 μm with a bandwidth from 3.2-3.7 μm. On the other hand, the strong cyano (CN) absorption peak occurs at ~4.48 μm and isothiocyanato (NCS) polar group has a broad and strong absorption in the 4.5-5.2 μm spectral regions.

The molecular vibration frequency (ω) depends on the spring constant (κ) and reduced mass (μ) of the diatomic group as:

$$\omega = \sqrt{\kappa / \mu} \tag{9}$$

As the reduced mass increases, the vibration frequency decreases, i.e., the absorption band shifts toward a longer wavelength. To prove this concept, a perdeuterated (~95% ^2H) 5CB (4'-pentylbiphenyl-4-carbonitrile) compound, designated as D5CB, has been developed. The carbon-deuteron (CD) absorption peak shifts from 3.5 μm to 4.6 μm. To ensure a low absorption in the desired MWIR window, we need to shift the absorption band further out to longer wavelength IR region. To do so, we need to replace hydrogen with a still heavier atom, such as fluorine. However, heavy fluorination would result in high melting point (T_m), large heating enthalpy (ΔH) and no nematic phase while partial fluorination might have severe vibration absorption. Therefore, a delicate balance between physical properties and absorption loss should be considered. In this report, we outline our molecular design strategy and demonstrate a first partially fluorinated LC compound to clean up the MWIR absorption bands, while exhibiting a nematic phase (although only about 2°C), high birefringence (Δn~0.2), a low visco-elastic coefficient (γ_1/K_{33}), and a modest dielectric anisotropy ($\Delta\varepsilon$= -2.7).

3.4.2 Molecular design strategy

In order for a compound to exhibit a nematic phase, it ought to have certain flexibility and aspect ratio. Based on the IR absorption spectra, the CH bonds in a phenyl ring have a much weaker and narrower absorption than those in the flexible alkyl chain. To further validate this concept, Compounds 1, 2, 3 and 4 (listed in Table 9) were prepared, dissolved in CCl_4 at a concentration of ~$5x10^{-5}$ mol/ml and then filled in a NaCl cell with 0.5-mm cell gap. The transmission spectra of the compounds were normalized to that of CCl_4. As illustrated in Fig. 14, both 1CB (4'-methylbiphenyl-4-carbonitrile) and 5CB exhibit a much broader and stronger absorption near λ= 3.4 μm than FB (#3, 4,4'-difluorobiphenyl) does. Indeed the CH bonds in the alkyl chain have a stronger absorption near λ= 3.4 μm than

the CH bonds in the phenyl rings. 5CB has a longer alkyl chain with more CH bonds in $-CH_2-$ and $-CH_3$ structures. Therefore, its absorption near 3.4 μm is much stronger. The absorption from C≡N (4.48 μm) in 1CB and 5CB is almost the same because of similar concentration. Compound #4 (F7CB) is a fluorinated 7CB and its absorption at ~3.4μm is significantly reduced since all the C-H bonds in the alkyl chain have been replaced by C-F bonds. It is known that $-CF_2-$ and $-CF_3$ have a broad and strong absorption in 7.1-9.5 μm, while the relatively weak absorption at ~4.25 μm is an overtone of the strong C-F vibration centered near 8.5 μm. This overtone can be further reduced by decreasing the number of CF groups, i.e., employing a shorter fluorinated alkyl chain. With a long perfluorinated alkyl chain, F7CB does not exhibit any mesogenic phase. Rather, its melting point is ~120°C (c.f. 30°C for 7CB) and its ΔH is increased dramatically so that its solubility in an LC host is limited to <5 wt%.

Table 9 Chemical structures and properties of the compounds studied. Cr stands for crystalline, N for nematic, and I for isotropic phase.

Compound #.	Chemical Structure	Abbreviation	PTT (°C)	ΔH (cal/mol)
1	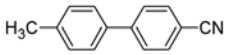	1CB	Cr109N(45)I[a]	5400
2	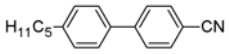	5CB	Cr24N35.3I	4100
3	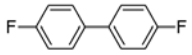	FB	Cr88I	2198[b]
4	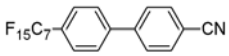	F7CB	Cr120.4I	10719
5	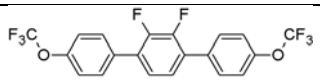	FT	C85.8N87.6I	4921

[a]( ) indicates a monotropic phase. [b]Enthalpy of sublimation

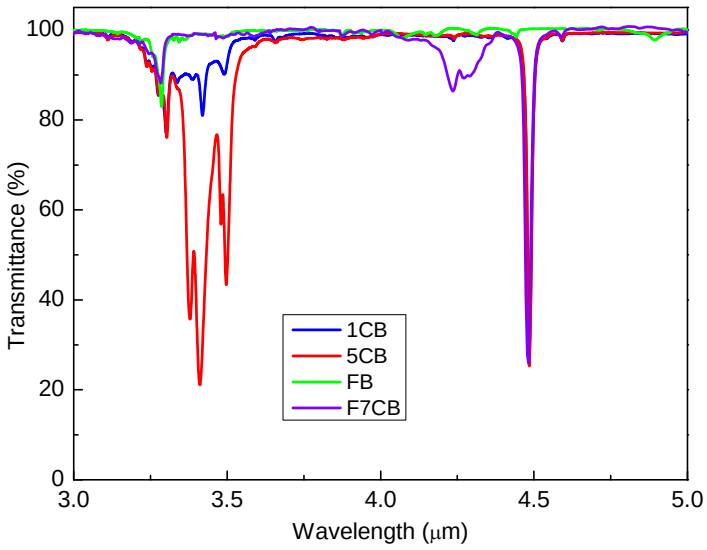

Fig. 14 Measured transmission spectra of 5CB (Red), 1CB (Blue), FB (Green) and F7CB (Violet).

Therefore, an alternative solution is to substitute only the CH bonds in the alkyl chain while keeping the core structure unaltered. Moreover, the fluorinated alkyl chain should not be too long, otherwise, the LC phase would be suppressed and the C-F vibrational overtone grows. Meanwhile, two or three phenyl rings are needed to ensure a high birefringence. To realize a useful electro-optic effect, the compounds should be polar with a modest Δε. To

replace CN, we could choose –F, -CF_3, or -OCF_3 as polar groups. Based on these concepts, we have synthesized a new partially fluorinated terphenyl compound (#5, abbreviated as FT) and evaluated its properties.

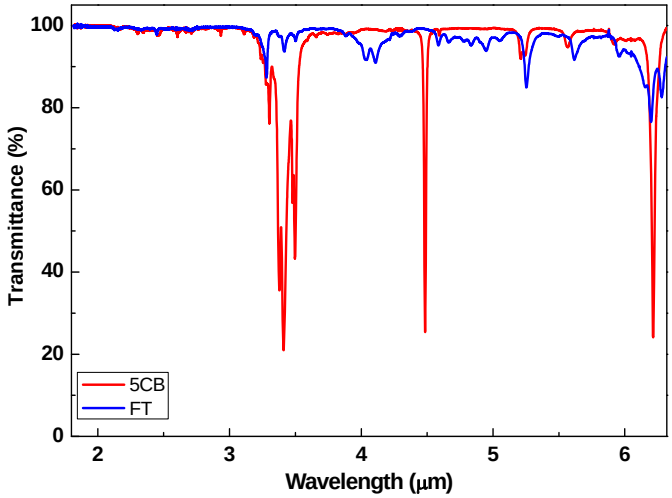

Fig. 15 Measured transmission spectra of 5CB (red line) and FT (blue line) in MWIR region

3.4.3 Results

As shown in Fig. 15, the absorption of FT at λ~3.4 μm is significantly reduced, compared to that of 5CB. Only a small absorption exists due to the residual CH bonds in the phenyl rings. The fairly weak absorption at λ~4 μm is the overtone of C-F stretching vibration. Overall, from 3 μm to 5 μm, the absorption is quite clean. Note that the absorption peak due to the C-O single bond stretching vibration is shifted to the wavelength longer than 7.5μm, which is out of MWIR window. For MWIR application, glass substrate and indium-tin-oxide (ITO) electrode are not quite transparent. Instead, we can use germanium substrate due to its low loss and high electrical conductivity. Besides, the LC alignment layer is usually very thin (~80 nm) which will not cause much absorption.

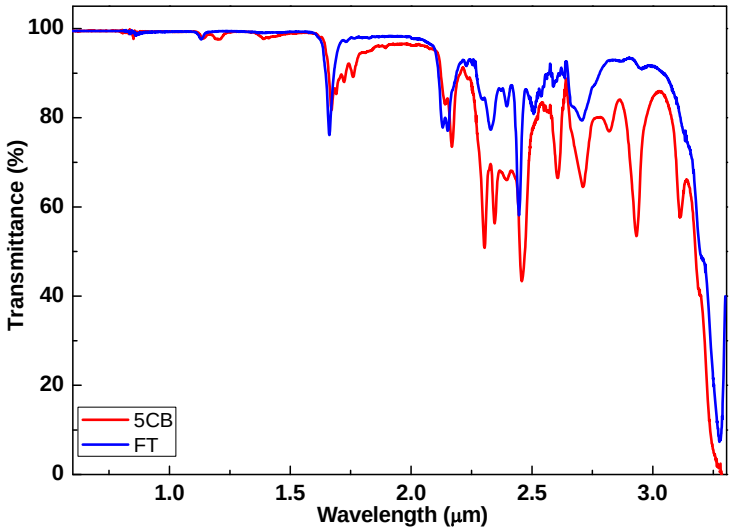

Fig. 16 Measured transmission spectra of 5CB (red line) and FT (blue line) in near IR region.

We also compared the absorption spectrum of FT with 5CB in the 0.6-3.2 μm range. Since the absorption is relatively small in this spectral region, a 2-mm-thick quartz cell was used and the concentrations for both compounds were increased to $5x10^{-4}$ mol/ml in CCl_4. A Cary UV/Vis/NIR spectrophotometer was employed to record the near IR transmission spectra. In Fig. 16, the blue and red lines represent the transmission spectra for FT and 5CB, respectively. The overall outcome is that some overtone absorption bands appear in this region, but FT exhibits a much higher transmittance than 5CB. In the spectral range of 2.2-3.0 μm, where the absorption is due to

the combination of C-H stretching, FT shows much weaker absorption than 5CB does. In addition, the λ~1.7 μm band resulting from the second harmonic of the 3.4-μm CH band becomes narrower for FT.

The physical properties of FT have also been characterized. From DSC measurements, FT exhibits a narrow (~2°C) but enantiotropic nematic phase from 85.8 °C to 87.6°C. To measure Δn, we doped FT into a negative $\Delta\varepsilon$ LC host, MLC-6882 (Merck, γ_1/K_{33}=6.75 ms/μm^2). The Δn of FT was extrapolated approximately by weight ratio and the resulting Δn~0.205 (λ=632.8 nm). According to the birefringence dispersion of liquid crystals, Δn decreases with wavelength and gradually saturates in the near IR region. In the MWIR region, the estimated Δn is ~0.18. At the edge of C-H absorption band, say λ=3.5μm, the estimated transmission of 5CB layer with 2π phase retardation is only 6.2%, but increases to 93% for the FT LC with the same phase retardation. The extrapolated $\Delta\varepsilon$ of FT is -2.71. The γ_1/K_{33} reduced as we doped 10% or 15% FT of FT into MLC-6882, indicating that FT has a somewhat lower γ_1/K_{33} than MLC-6682. Such a low viscosity originates from the –OCF_3 group.

3.4.5 Future plan

The FT compound we proposed serves as an important first example for future development of low-loss MWIR liquid crystals for amplitude or phase modulation. With additional molecular design and synthesis, e.g., substituting fluoro groups in different positions of the phenyl rings or employing –OCF_3 at one phenyl ring terminal as a polar group, a positive Δε and potentially wider nematic range will result. In order to further widen the nematic range for room temperature operation, several compounds have to be developed in order to formulate eutectic mixtures. As illustrated in Fig. 17, the general molecular structure shows some compounds which not only satisfy the low-loss criterion but also have potential for wider temperature range. However, the phase transition temperature of a compound is difficult to predict before it is synthesized.

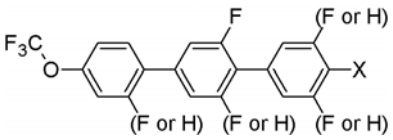

Fig. 17 Molecular structure with potentially wider nematic range for forming eutectic mixtures (X=F or OCF_3).

4. Personnel Supported

One post doctorate and 2 graduate students.

5. Publications: (3/1/2009 to 2/28/2014)

1. K. M. Chen, H. Ren, and S. T. Wu, "PDLC-based VOA with a small polarization dependent loss," Opt. Commun. 282, 4374-4377 (Nov. 2009).
2. J. Sun, H. Xianyu, S. Gauza, and S. T. Wu, "High birefringence phenyl tolane positive compounds for dual frequency liquid crystals," Liquid Crystals 36, 1401–1408 (Dec. 2009).
3. L. Rao, Z. Ge, and S. T. Wu, "Viewing angle controllable displays with a blue-phase liquid crystal cell," Opt. Express 18, 3143- 3148 (Jan. 2010).
4. M. Jiao, Y. Li, and S. T. Wu, "Low voltage and high transmittance blue-phase liquid crystal displays with corrugated electrodes," Appl. Phys. Lett. 96, 011102 (Jan. 2010).
5. K. M. Chen, S. Gauza, H. Xianyu, and S. T. Wu, "Submillisecond gray-level response time of a polymer-stabilized blue phase liquid crystal," J. Display Technology 6, 49-51 (Feb. 2010).
6. J. Yan, H. C. Cheng, S. Gauza, Y. Li, M. Jiao, L. Rao, and S. T. Wu, "Extended Kerr effect in polymer-stabilized blue-phase liquid crystals," Appl. Phys. Lett. 96, 071105 (Feb. 2010).
7. Q. Song, S. Gauza, H. Xianyu, S. T. Wu, Y. M. Liao, C. Y. Chang, and C. S. Hsu, "High birefringence lateral difluoro phenyl tolane liquid crystals," Liq. Cryst. 37, 139-147 (Feb. 2010).
8. J. Yan, M. Jiao, L. Rao, and S. T. Wu, "Direct measurement of electric-field-induced birefringence in a polymer-stabilized blue-phase liquid crystal composite," Opt. Express 18, 11450-11455 (May 2010)
9. S. Xu, Y. Liu, H. Ren, and S. T. Wu, "A novel adaptive mechanical-wetting lens for visible and infrared imaging," Opt. Express 18, 12430-12435 (June 2010) (This paper was highlighted in the cover page)

10. K. M. Chen, S. Gauza, H. Xianyu, and S. T. Wu, "Hysteresis effects in blue-phase liquid crystals," J. Display Technology 6, 318-322 (Aug. 2010)
11. H. Ren, H. Xianyu, and S. T. Wu, "Liquid crystal droplet array for non-contact electro-optic inspections," J. Phys. D: Appl. Phys. 43, 365103 (Aug. 2010).
12. H. Ren and S. T. Wu, "Optical switch using a deformable liquid droplet," Opt. Lett. 35, 3826-3828 (Nov. 2010).
13. H. Xianyu, X. Liang, J. Sun and S. T. Wu, "High performance dual frequency liquid crystal compounds and mixture for elevated temperature operation," Liq. Cryst. 37, 1493-1499 (Dec. 2010).
14. H. Ren, S. Xu, D. Ren, and S. T. Wu, "Novel optical switch with a reconfigurable dielectric liquid droplet," Opt. Express 19, 1985-1990 (Jan. 2011). (This paper was highlighted in the cover page)
15. S. Xu, H. Ren, Y. Liu, and S. T. Wu, "Dielectric liquid microlens with switchable negative and positive optical power," IEEE J. MEMS 20, 297-301 (Feb. 2011).
16. H. C. Cheng, S. Xu, Y. Liu, S. Levi, and S. T. Wu, "Adaptive mechanical-wetting lens actuated by ferrofluids," Opt. Commuin. 284, 2118-2121 (April, 2011).
17. H. Ren, S. Xu, Y. Liu, and S. T. Wu, "Electro-optical properties of dielectric liquid microlens," Opt. Commuin. 284, 2122-2125 (April, 2011).
18. Y. Chen, H. Xianyu, J. Sun, P. Kula, R. Dabrowski, S. Tripathi, R. J. Twieg, and S. T. Wu, "Low absorption liquid crystals for mid-wave infrared applications," Opt. Express 19, 10843-10848 (May, 2011)
19. H. Ren and S. T. Wu, "Fringing field stretching of a pillared liquid crystal droplet," J. Phys. D: 44, 375301 (Aug. 2011).
20. Y. Chen, J. Sun, H. Xianyu, S. T. Wu, X. Liang, and H. Tang, "High birefringence fluoro-terphenyls for thin-cell-gap TFT-LCDs," J. Display Technol. 7, 478-481 (Sept. 2011).
21. H. Ren, S. Xu, and S. T. Wu, "Voltage-expandable liquid crystal surface," Lab Chip 11, 3426-3430 (Sept. 2011). (Back cover page)
22. Y. Liu, H. Ren, S. Xu, Y. Chen, L. Rao, T. Ishinabe, and S. T. Wu, "Adaptive focus integral image system design based on fast-response liquid crystal microlens," J. Display Technol. 7, 674-678 (Dec. 2011).
23. H. Ren, S. Xu, and S. T. Wu, "Optical switch based on variable aperture," Opt. Lett. 37, 1421-1423 (May 2012).
24. S. Xu, H. Ren, Y. Liu, and S. T. Wu, "Color displays based on voltage-stretchable liquid crystal droplet," J. Display Technol. 8, 336-340 (June 2012).
25. S. Xu, H. Ren, J. Sun, and S. T. Wu, "Polarization independent VOA based on dielectrically stretched liquid crystal droplet," Opt. Express 20, 17059-17064 (July 2012).
26. H. Ren, S. Xu, Y. Liu, and S. T. Wu, "Liquid-based infrared optical switch," Appl. Phys. Lett. 101, 041104 (July 2012).
27. J. Sun, Y. Chen, and S. T. Wu, "Submillisecond-response and scattering-free infrared liquid crystal phase modulators," Opt. Express 20, 20124-20129 (Aug. 2012).
28. H. Ren, S. Xu, and S. T. Wu, "Gradient polymer network liquid crystal with a large refractive index change," Opt. Express 20, 26464-26472 (Nov. 2012). (This paper was chosen as "Image of Week" at OSA InfoBase).
29. S. Xu, H. Ren, and S. T. Wu, "Adaptive lens actuated by liquid crystal pistons," Opt. Express 20, 28518-28523 (Dec. 2012). (This paper was chosen as "Image of Week" at OSA InfoBase).
30. H. Ren, S. Xu, and S. T. Wu, "Liquid crystal pump," Lab. Chip 13, 100-105 (Jan. 2013). (Back cover page)
31. H. Ren, S. Xu, Y. Liu, and S. T. Wu, "Switchable focus using a polymeric lenticular microlens array and a polarization rotator," Opt. Express 21, 7916-7925 (March 2013).
32. J. Sun, S. Xu, H. Ren, and S.T. Wu, "Reconfigurable fabrication of scattering-free polymer network liquid crystal prism/grating/lens," Appl. Phys. Lett. 102, 161106 (April 2013).
33. H. Ren, S. Xu, and S. T. Wu, "Polymer-stabilized liquid crystal microlens array with large dynamic range and fast response time," Opt. Lett. 38, 3144-3147 (Aug. 2013).
34. H. Ren, S. Xu, Y. Liu, and S. T. Wu, "Plano-convex/Biconvex microlens array based on self-assembled photocurable polymer droplets," J. Mater. Chem. C 1, 7453-7458 (Oct. 2013).
35. (Topical Review) S. Xu, H. Ren, and S. T. Wu, "Dielectrophoretically tunable optofluidic devices," J. Phys. D: Appl. Phys. 46, 483001 (Nov. 2013).
36. H. Ren, S. Xu, Y. Liu, and S. T. Wu, "Optically anisotropic microlens array film directly formed on a single substrate," Opt. Express 21, 29304-29312 (Dec. 2013).
37. J. Sun, S.T. Wu, and Y. Haseba, "A low voltage submillisecond-response polymer network liquid crystal spatial light modulator," Appl. Phys. Lett. 104, 023305 (Jan. 13, 2014).

38. H. Zhang, H. Ren, S. Xu, and S.T. Wu, "Temperature effects on dielectric liquid lenses," Opt. Express 22, 1930-1939 (Jan. 27, 2014).
39. (Review paper) J. Sun, and S.T. Wu, "Recent advances in polymer network liquid crystal spatial light modulators," J. Polym. Sci., Part B: Polym. Phys. 52, 183-192 (Feb. 1, 2014).

6. Interactions or Transitions: (3/1/2009-2/28/2014)

A. Presentations at conferences or research institutes:

1. S. T. Wu, "The dawn of blue-phase LCD"
   (Plenary) Conference on Liquid Crystals, Mikołajki, Poland (Sept. 16-20, 2013)
2. S. T. Wu, "Polymer-stabilized blue-phase LCDs"
   (Tutorial) International Meeting on Information Display, Daegu, Korea (Aug. 26-29, 2013)
3. S. T. Wu, "Is blue-phase LCD ready for prime time?"
   (Plenary talk) Symposium on Liquid Crystal Photonics, Chengdu, China (April 20-21, 2013).
4. S. T. Wu, "Submillisecond-response and scattering-free polymer network liquid crystals,"
   (Invited talk) ACS Annual Meeting, New Orleans (April 7-9, 2013).
5. S. T. Wu, "Blue-phase liquid crystal displays,"
   (Keynote) Photonics West, San Francisco, Feb. 5, 2013 (2013).
6. S. T. Wu, "Microsecond-response-time blue-phase LCDs,"
   (Tutorial Seminar) SID Annual Meeting, Boston, MA (June 4, 2012).
7. S. T. Wu, "Blue-phase LCD: A disruptive technology?"
   (Plenary talk) Symposium on Liquid Crystal Photonics, Guilin, China (March 24-25, 2012).
8. S. T. Wu, "The dawn of blue-phase LCDs,"
   (Plenary talk) Taiwan LC Society annual meeting (Feng Chia University, Taichung, Taiwan, Dec. 16, 2011)
9. S. T. Wu, "Blue-phase LCDs",
   (Seminar M13) SID annual meeting (Los Angeles, CA, May 16, 2011)
10. S. T. Wu, "Adaptive liquid and liquid crystal lenses",
    (Invited talk) ECE Department, University of Wisconsin @ Madison (May 2, 2011)
11. S. T. Wu, "Optically-isotropic liquid crystals for photonics and display applications",
    (Plenary talk) Int'l Liquid Crystal Photonics Conference (Hong Kong, Dec. 6-8, 2010)
12. S. T. Wu, "Submillisecond-response polymer network liquid crystals,"
    (Invited talk) MRS Fall Meeting (Boston, MA. Nov. 29-Dec. 1, 2010)
13. S. T. Wu, "Submillisecond-response liquid crystal photonic devices,"
    (Plenary talk) 3rd Int'l Liquid Crystal Photonics Conference (Elche, Spain, Sept. 8-10, 2010)
14. S. T. Wu, "Emerging LCDs based on the Kerr effect",
    (Tutorial talk) 23rd Int'l Liquid Crystal Conference (Krakow, Poland, July 11-16, 2010)
15. S. T. Wu, "Emerging blue phase LCDs",
    (Plenary talk) FPD China (Shanghai, China: March 16-17, 2010)
16. S. T. Wu, "Low voltage polymer-stabilized blue phase LCDs",
    (Plenary talk) Taiwan LC Society Annual Meeting, (Hsinchu, Taiwan, Dec. 18, 2009)
17. S. T. Wu, "Tunable-focus lenses",
    (Plenary talk) 12th Polymer Material Topical Conference, (Taipei, Taiwan, Nov. 11, 2009)
18. S. T. Wu, "Emerging LCDs based on Kerr Effect,"
    (Plenary talk) 13th Topical Conference "Optics of Liquid Crystals", (Erice, Italy, Sept. 28-Oct. 2, 2009)
19. S. T. Wu, "Enhancing the energy efficiency of TFT LCDs",
    (Invited talk) SID Annual Meeting, (San Antonio, Texas, June 4, 2009)
20. S. T. Wu, "Energy efficient TFT LCDs",
    (Seminar M1) SID Annual Meeting, (San Antonio, Texas, June 1, 2009)
21. S. T. Wu, "Energy efficient liquid crystal displays",
    (Short Course) Asia Display/IDMC (Taipei, Taiwan, April 27, 2009)

B. Transitions:

We have delivered some high performance LC mixtures containing the compounds developed in this report to Raytheon, Teledyne, Kent Optronics Inc. (KOI), and Nova Photonics for their device testing. The contact persons are listed as follows:

Raytheon: Dr. Terry Dorschner (Laser beam steering) (Retired in 2013)
Email: tadorschner@gmail.com

Teledyne: Dr. Dong-Feng Gu (Advanced tunable filters)
Email: dgu@teledyne.com (Tel: 805-373-4707)

KOI: Dr. Le Li (Electronically switchable IR beam splitter)
Email: leli@kentoptronics.com (Tel: 845-897-0138 x 101)

Nova Photonics: Dr. Fred Levinton (Tunable optical filters)
Email: flevinton@novaphotonics.com (Tel: 609-243-3463)

7. Honors and Awards

Prof. Wu is a recipient of OSA Esther Hoffman Beller Medal (2014), SID Slottow-Owaki Prize (2011), OSA Joseph Fraunhofer award/ Robert M. Burley Prize (2010), SPIE G. G. Stokes Award (2008), and SID Jan Rajchman Prize (2008). He was the founding Editor-In-Chief of IEEE/OSA Journal of Display Technology. He has co-authored 7 books, 440 journal papers, and obtained 79 U.S. patents. He is a Charter Fellow of the National Academy of Inventors (NAI), and a Fellow of the IEEE, OSA, SID and SPIE. Presently, he is serving as Chair of OSA Publications Council, OSA Board of Directors, SID Honors and Awards Committee, and SPIE Stokes Award Committee.